文章编号 1672-6634(2018)03-0038-08 DOI 10.19728/j.issn1672-6634.2018.03.007

# Dependence of Photoluminescence Properties of $Y_6WO_{12}$ : $Eu^{3+}$ Phosphors on Microstructure and Crystal Structure①

LI Huai-yong FANG Lu LI Miao-miao SUN Wen-zhi WEI Deng-hu
LI Yan MA Kang-xi WANG Ya-hao

(School of Materials Science and Engineering, Liaocheng University, Liaocheng 252059, China)

**Abstract** Polycrystalline $Y_6WO_{12}$ : $Eu^{3+}$ phosphors in cubic and rhombohedral phases were synthesized by using a citrate-complexation method. The structural and photoluminescence(PL) properties of the as-prepared phosphors were characterized by powder X-ray diffraction(XRD), Raman, stable-state PL and temporal decay. It was revealed that the phosphors in both cubic and rhombohedral phases could be excited by near-UV and blue light via $WO_6$ groups and $Eu^{3+}$ ions, respectively. However, the $WO_6$ groups show no luminescence at room temperature, and the PL is dominated by the red-emitting of $Eu^{3+}$ ions $^5D_0$-$^7F_2$ or $^5D_0$-$^7F_1$ transition. At the same time, the PL excitation, emission and temporal decay spectra of the phosphors vary systematically with the calcination temperature as well as the crystal structure. The evolution was discussed from the standing point of the local environment of $W^{6+}$ and $Eu^{3+}$ ions.

**Key words** tungstates; europium ion; red luminescence; energy transfer

**CLC** O644.1 **Document code** A

## 0 Introduction

Combinations of near-UV/blue LED and (blue, green and red)/(green and red) /(yellow) color-conversion phosphors are efficacious approaches to generate white light[1-3]. The widely used combination of a blue LED chip and yellow phosphor YAG:$Ce^{3+}$ has a low color rendering index and a high correlated color temperature[4]. A solution to this problem is using a near-UV LED chip and blue ($BaMgAl_{10}O_{17}$ : $Eu^{2+}$), green ($ZnS$:$Cu^+$, $Al^{3+}$) and red ($Y_2O_2S$:$Eu^{3+}$) phosphors together[5,6]. However, the red phosphor ($Y_2O_2S$:$Eu^{3+}$) has some serious drawbacks in terms of low absorption efficiency of near-UV/blue light in the range of 320-470 nm and poor stability under near-UV radiation. Therefore near-UV/blue light excited red color-conversion phosphors were investigated extensively in recent years[7,8], including a series of $Eu^{3+}$ ions activated tungstates.

Tungstates have outstanding advantages, such as easy to be synthesized, stable to UV radiation, and capable of absorbing near-UV light in a wide range of wavelength depending on the crystal structure[9]. These features make tungstates promising hosts for near-UV/blue light excited red color-conver-

① 收稿日期:2018-08-06
基金项目:国家自然科学基金项目(51302125,51802137);山东省自然科学基金项目(ZR2017QB017);聊城大学大学生科技文化创新基金项目(26312171913,26312171920)资助
通讯作者:李怀勇,男,汉族,博士,讲师,研究方向:发光材料,E-mail:lihuaiyong@lcu.edu.cn.

sion phosphors. Among the tungstate hosts, compounds having a chemical formula of $R_6WO_{12}$ (R could be Y and lanthanum elements) have been widely investigated. Beaury and co-workers firstly reported the PL properties of $Eu^{3+}$ ion-activated $Y_6WO_{12}$[10]. Li et al. reported the electronic structure and PL properties of the tungstate and its solid solutions with molybdate, $Y_6W_xMo_{1-x}O_{12}:Eu^{3+}$[11,12]. Most recently, the PL properties of $Y_6WO_{12}$ activated with $Eu^{3+}$, $Sm^{3+}$, $Dy^{3+}$, $Tb^{3+}$, and $Tm^{3+}$ were extensively studied[13-18]. It is revealed that the tungstate host could act as a sensitizer to the doped luminescent center, the energy transfer from host lattice to luminescent centers is efficacious, and $Y_6WO_{12}$ is a promising host for phosphors for solid-state lighting.

The crystal structure and structural transformation in $Y_6WO_{12}$ and other analogues compounds have also been intensively investigated[19]. It was revealed that the tungstates of Tb to Lu, and Y crystallize in a rhombohedral phase[20] and $Y_6WO_{12}$ undergoes a structural transformation from the rhombohedral phase to a high temperature cubic phase[21,22]. Recently, it was reported that $Y_6WO_{12}$ in a cubic phase (low temperature cubic phase) could be obtained by wet-chemical method[23-25]. According to the literature, $Y_6WO_{12}$ within cubic fluorite phase could be synthesized at temperatures as low as 600℃ and 750℃, respectively, depending on the synthesis parameters[23,25]. Also, the temperature of the phase transformation from cubic to rhombohedral phase was revealed to vary around 1 200℃. While the PL properties of $Eu^{3+}$ ion-activated $Y_6WO_{12}$ in cubic phase have not been reported, the differences in the PL properties and the evolution of the PL properties of $Y_6WO_{12}$ with the crystal structure are not known.

In this work, $Eu^{3+}$ ions-doped $Y_6WO_{12}$ powders were synthesized by using a citrate-complex method, the obtained precursors were then calcined at different temperatures ranging from 800℃-1 300℃ to modify the crystal structure and microstructure of the hosts. The structural and PL properties were comparatively studied. The variations in the PL spectra and temporal decay are discussed from the structural standing point.

## 1 Experimental method

The starting materials $Y(NO_3)_3$ (99.99%), $Eu(NO_3)_3$ (99.99%), $(NH_4)_{10}H_2(W_2O_7)_6$ (99.99%), and $C_6H_8O_7$ (>99.5%) were purchased from Sigma-Aldrich, and used without further purification. Powder samples were synthesized from a citrate-complex precursor. The detailed synthesis procedure can be found elsewhere[12]. The powder was divided into five patches and then calcined at a gradually increased temperature from 800℃-1 300℃ with an interval of 100℃ for 4 hours in air to get the final products, which were referred to S1 to S6, respectively.

The structural characteristics of the powders were examined by using powder XRD and Raman measurements. The XRD patterns was collected on a Philips X'Pert MPD X-ray diffraction system at 40 kV, 30 mA and Cu Karadiation (=1.540 56 Å) as incident beam. The range was from 20°-80° (2) with a step length of 0.02° (2). The Raman measurement was performed on a JASCO NRS-3300 laser Raman spectrophotometer with an Argon laser (532 nm) as excitation. The data were scanned over a range of 112-1 229 $cm^{-1}$ with a resolution of 4.2 $cm^{-1}$. The steady PL spectra and PL lifetime were collected on a PTI fluorescence spectrophotometer. A 60 W Xe-arc lamp was used as the excitation light source for the steady PL measurement, and a 25 W Xe-flash lamp for PL lifetime measurements. All the measurements were performed at room temperature in air.

## 2 Results and discussions

In this work, $Eu^{3+}$ ions-doped $Y_6WO_{12}$ powders were synthesized by using a citrate-complex method, the XRD patterns of the powders calcined at different temperatures are shown in Figure 1. It is observed

that when the powder was calcined at 1 300℃ (S6), the rhombohedral is obtained, while at temperatures of and below 1 200℃ (S5-S1), the cubic phase is obtained, which agree well with previous work[23,25]. The diffraction peaks of the rhombohedral and the cubic phases agree well with the Joint Committee on Powder Diffraction Standards (JCPDS) file Nos. 20-1420 and 35-0174, respectively. No diffraction peak other than the JCPDS cards was observed, indicating the rhombohedral and the cubic phases are structural pure. For the cubic phase, a gradually broadening in the diffraction peaks with the decreasing of the calcination temperature was observed.

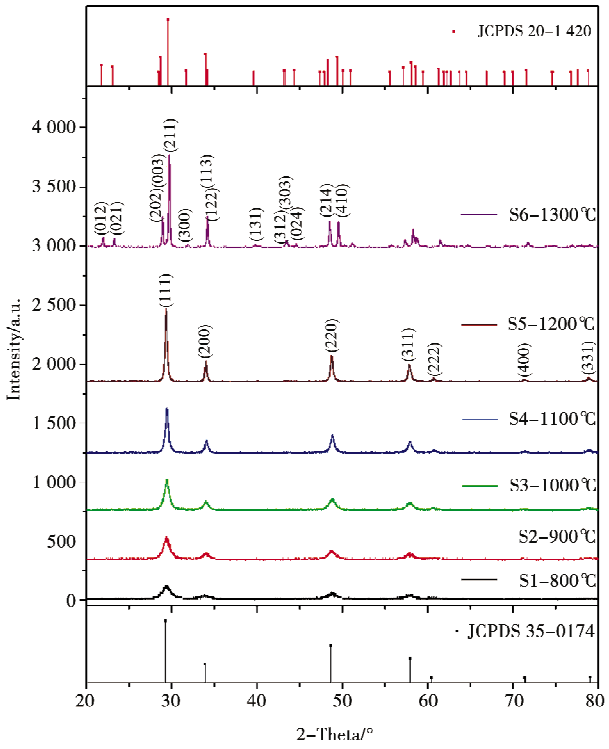


**Figure1 XRD patterns of $Y_6WO_{12}$:Eu, powders as a function of calcination temperature, and the JCPDS cards of $Y_6WO_{12}$ within cubic and rhombohedral phases**

It is generally accepted that the broadening of XRD diffraction peaks might be caused by the decreasing of crystallite size ($XS$) and the lattice strain, which can be obtained from the XRD diffraction patterns by working with Williams-Hall equation shown as following

$$XS = \frac{0.9\lambda}{\beta\cos\theta - 4\varepsilon\sin\theta}, \qquad (1)$$

where $\beta$ is the full width half maximum (FWHM) of the diffraction peaks, $\theta$ is the Bragg angle, and $\lambda$ is the wavelength of the incident beam. In our cases, the data of (111), (200), (220), (311), (222), and (400) diffraction peaks were used to work with Eq. 1. The estimated crystallite sizes and lattice strains are shown in Figure 2. The crystallite size was found to increase from 83 nm to 399 nm with the calcination temperature. The lattice strain on the contrary decreases from 0.379 to 0.030. This result was ascribed to a fast diffusion of the ions, reduce of lattice defects and merge of small crystallites at high calcination temperature.

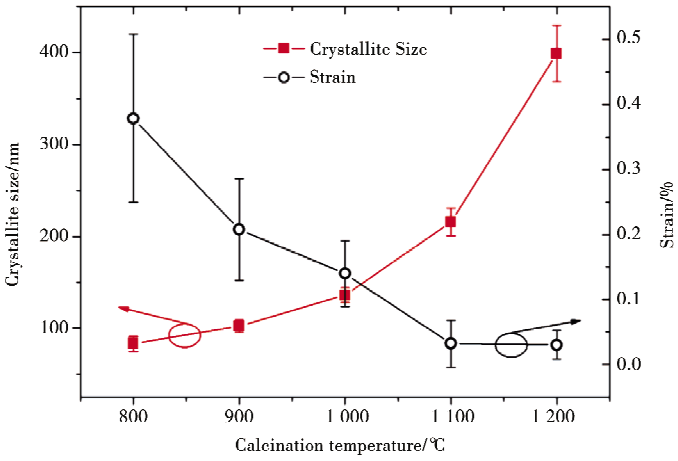


**Figure 2 Crystallite size and lattice strain of $Y_6WO_{12}$:Eu, powders as a function of calcination temperature**

The Raman spectra of the as-prepared samples S6-S2 are shown in Figure 3, which are distinctly divided into two groups, namely, rhombohedral and cubic according to the XRD patterns. The spectrum of the rhombohedral phase is relatively more abundant that those of the cubic phase. The structure of rhombohedral $Y_6WO_{12}$ has been well determined. According to Diot et al., the rhombohedral $Y_6WO_{12}$ structure can be described by R $\bar{3}$ space group with $R$-centered setting[19]. In the cell, W takes an octahedral site; Y takes 6$f$ Wyckoff site (with $C_1$ point symmetry) and bonds to seven O atoms, forming a distorted monocapped trigonal prism. However, we know less about the cubic structure of these compounds, including the cations and anions arranged in some distorted fluorite type in the cell. The spectrum of S6 is in line with that of $Y_6WO_{12}$ reported by Gagarina et al[26].

**The peak at** 900-600 $cm^{-1}$ is due to the stretching vibrations of $WO_6$; 600-400 $cm^{-1}$ is due to the bending vibrations of $YO_7$ and $WO_6$; and below 400 $cm^{-1}$ corresponds to the deformation vibrations of the octahedral[26]. The spectra of S5-S2 in cubic phase are significantly different from that of S6 in rhombohedral phase. In these spectra, the peaks around 800 $cm^{-1}$ are very weak or unobservable, while the peaks at 600-800 $cm^{-1}$ are very strong. The discrepancy of these spectra implies that ideal octahedral $WO_6$ and ordered cations arrangement have not formed in the samples other than S6. As well known, in ideal fluorite cells, the ratio of the cations to anions is 1∶2, and the coordination numbers of the cations and anions are 8 and 4, respectively. While in $Y_6WO_{12}$, the ratio of cations and anions is 7∶12, which means that the cation vacancy, anion vacancy and cations disorder might coexist in the cell, and the 8-and 4-fold coordination for cations and anions might not be reached.

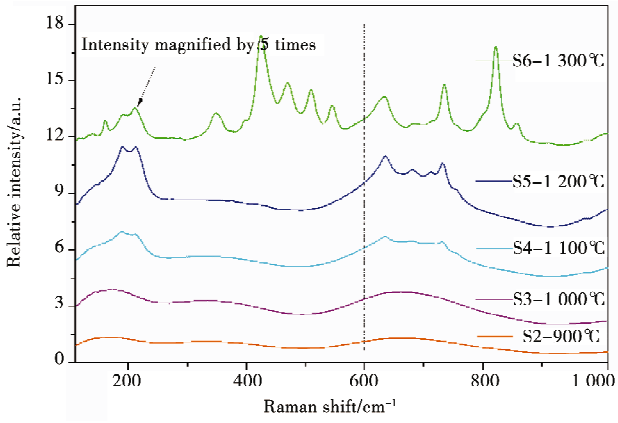


**Figure3　Evolution of the Raman spectra of $Y_6WO_{12}$: Eu with the calcination temperature**

Figure 4 shows the PL excitation spectra of $Y_6WO_{12}:Eu$ in cubic phase (S1-S5) as well as in rhombohedral phase (S6). The spectrum of the rhombohedral phase consists of a broad band centered at 309 nm with a shoulder ranging from 350-400 nm, and a series of lines around 394.0 nm and 464.8 nm, being consistent with the references[10,11,16,18]. The former is ascribed to the excitation of electron from filled O-2p to unoccupied W-5d orbitals in $WO_6$ groups, or from valence band to conductive band of the host lattice[11,27]. The latter is due to the excitation of electron in $Eu^{3+}$ ions from the ground state of $^7F_0$ configuration to $^5D_2$ and $^5L_6$ configurations within 4f-shell, respectively. In the isostructural molybdates $Y_6MoO_{12}$ host lattice, the charge transfer excitation between $O^{2-}$ and $Eu^{3+}$ was reported to have an isolated excitation band centered at 248 nm[12,28]. While in our situation, it might be overlapped with the excitation of $WO_6$ band and not observed. It is obviously that the excitation of $WO_6$ groups is far more efficient than the excitation of $Eu^{3+}$ ion f-f transition. This due to the fact that the transition from O-2p to W-5d orbitals within $WO_6$ groups is allowed while the transition within Eu-4f orbitals is spin and parity forbidden. It is also implied that the energy transfer form $WO_6$ groups to dopant $Eu^{3+}$ ions is efficient.

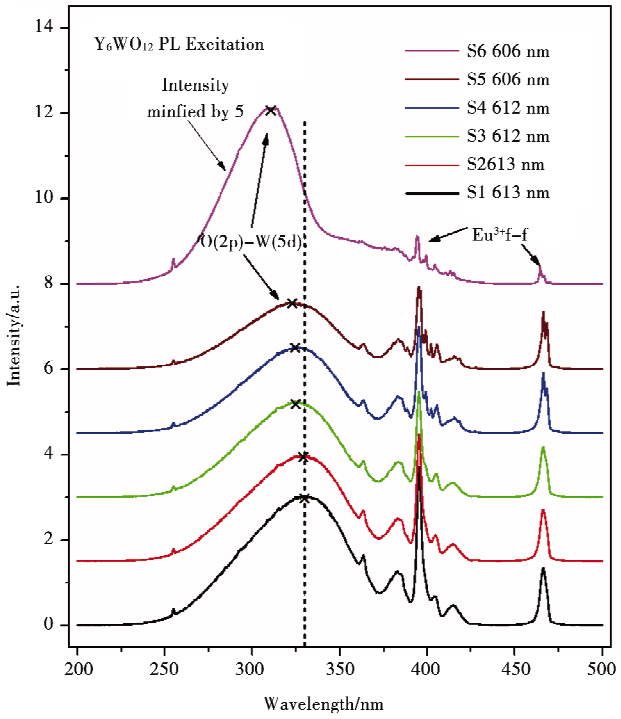


**Figure4　PL excitation spectra of $Y_6WO_{12}:Eu$ powders as a function of calcination temperature**

The components of the spectra in cubic phase are similar to those of the rhombohedral phase, viz., a broad band and a series of sharp lines. The differences are mainly in that the peak wavelength of the excitation band shift from 309 nm of the rhombohedral phase to about 328 nm of the cubic phase. The wavelengths of $^7F_0$-$^5D_2$ and $^7F_0$-$^5L_6$ transitions shift from 394.0 nm and 464.8 nm to 395.3 nm and 466.

8 nm, respectively. It is also viewed that the spectra of the cubic phase varies systematically with the calcination temperature. (1) The excitation intensities of both $WO_6$ groups and $Eu^{3+}$ ions intensify from S5 to S1. (2) The peak wavelength of $WO_6$ excitation band red-shifts gradually from 323 nm to 330 nm. (3) The f-f excitation lines become broadened and the fine-structure of the lines gets vague. These variations are considered to be triggered by the structure evolution induced by the processing.

Both $WO_6$ groups and $Eu^{3+}$ ions were excited to observe the emission characteristics, and the results are shown in Figure 5(a) and 5(b), respectively. The emission spectra of the cubic phase are comparably simple. There are five distinctive bands centered at 580.0 nm, 593.3 nm, 600.3 nm, 612.0 nm and 629.3 nm. The emission spectrum of S1 is dominated by the emission at 612.0 nm and 629.3 nm, which are due to the $^5D_0$-$^7F_2$ transition. With the increasing of crystallite size, the wavelength of line #1 shifts from 612.0 nm of S1 to 609.0 nm of S5, and that of line #2 shift from 629.3 nm to 632.0 nm. In other words, the splitting of $^7F_2$ energy level gets larger from S1 to S5. This indicates that the chemical environment evolves gradually from S1 to S5. As to the rhombohedral S6, the spectra are dominated by the emission due to $^5D_0$-$^7F_2$ transition at 606 nm, 608.8 nm, 617.8 nm, 632.5 nm and 634 nm. At the same time, the emissions due to $^5D_0$-$^7F_1$ at 583.5 nm, 588.5 nm and 603.3 nm, and $^5D_0$-$^7F_0$ at 578.0 nm are also very intensive. Comparing the spectra of the cubic and rhombohedral phases, it is revealed that the emission due to $^5D_0$-$^7F_1$ transition intensifies greatly when the $Y_6WO_{12}$ host lattice undergoes a structural transform from cubic to rhombohedral. The dominated emission shifts from 612.0 nm and 629.3 nm of the cubic phase to 606 nm and 603 nm of the rhombohedral phase.

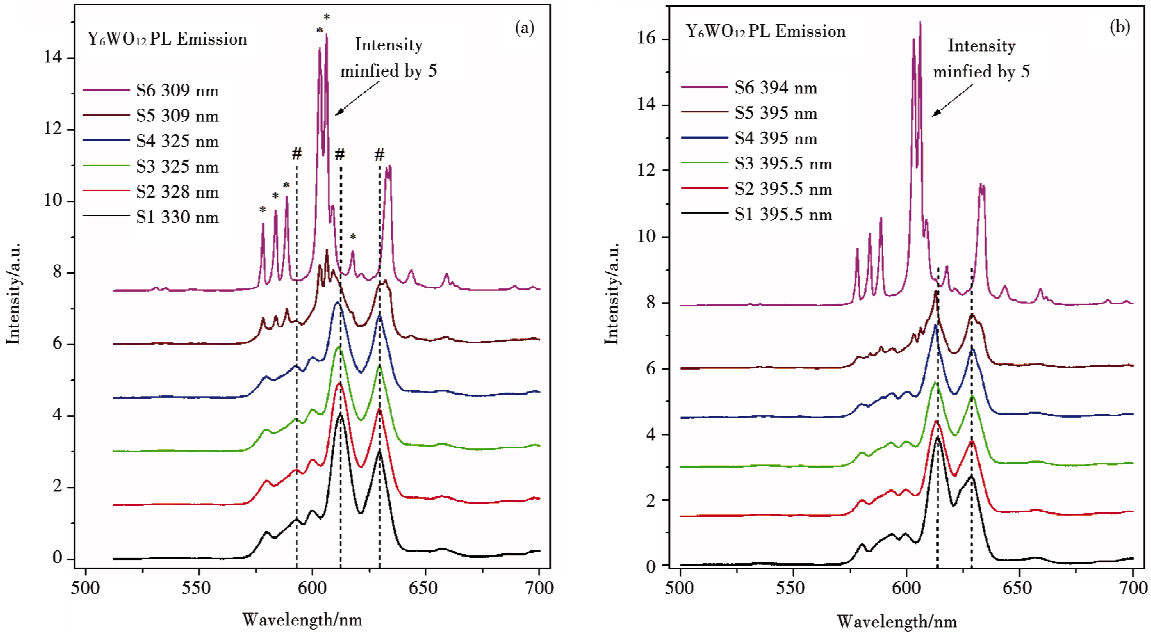


**Figure 5 PL spectra of $Y_6WO_{12}$:Eu powders as a function of calcination temperature**
**(a) Exciting into the host lattice and (b) into the $Eu^{3+}$ f-f transition**

The emission spectra of S5 are very interesting. The emission line corresponding to both rhombohedral (# peaks in Figure 5) and cubic (* peaks in Figure 5) phases are observed. This indicates that in S5 sample, $Eu^{3+}$ ions having two different chemical environments. Therefore the observed emission spectra are the overlap of two kinds of $Eu^{3+}$ ions. From the intensity ratio, it can be also deduced that the amount of $Eu^{3+}$ ions in rhombohedral-environment is far less than that in cubic-environment. This is due to the fact that at the identical concentration (2.5 mol%), the emission intensity of the rhombohedral phase is about 20 times stronger than the cubic phase. It is also suggested that although the long-range structure of the lattice is still of cubic, which can be confirmed from the XRD pattern, a re-ar-

rangement of the atoms starts at this calcination temperature. This confirms the conclusion that the structural transformation from cubic to rhombohedral is of diffusional nature[L25].

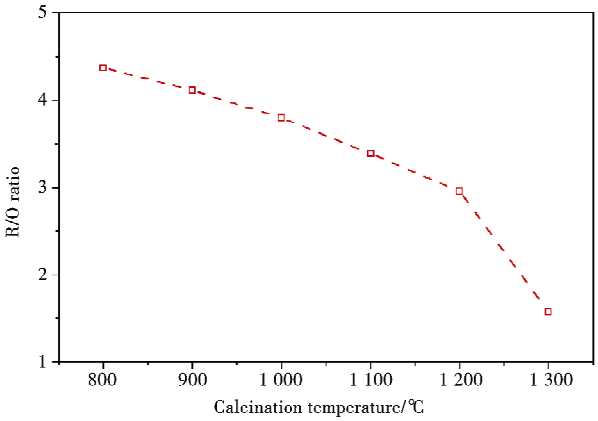


**Figure 6　R/O ratio of $Y_6WO_{12}:Eu$ powders as a function of the calcination temperature**

It has been mentioned that in the cubic phase the dominated emissions are at 613 nm and 629 nm, which due to $^5D_0$-$^7F_2$ transition, while in the rhombohedral phase, they are at 603 nm and 606 nm, which rises from the $^5D_0$-$^7F_1$ and $^5D_0$-$^7F_2$ transitions, respectively. Since the intensity of $^5D_0$-$^7F_2$ transition is hypersensitive to the deviation from centrosymmetry, the intensity ratio of $I(^5D_0$-$^7F_2)/I(^5D_0$-$^7F_1)$, which designed as R/O ratio, is commonly used as a measurement of the site symmetry. The R/O ratio of the $Eu^{3+}$ sensitized spectra are calculated and plotted in Figure 6. The R/O value decreases gradually from 800℃ to 1 200℃, and then suddenly from 1 200℃-1 300℃, corresponding to the phase transformation from cubic to rhombohedral. The variation of R/O ratio indicates that the symmetry of Y(Eu) site in the cubic phase gradually increases with the annealing temperature, and it is lower than that in the rhombohedral phase.

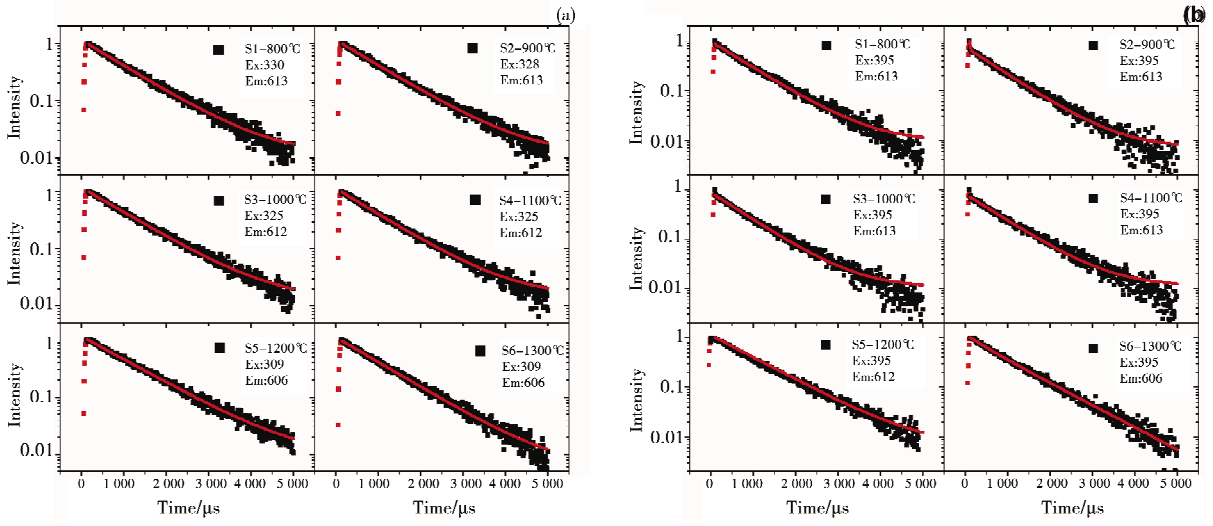


**Figure7　Luminescence decay data of $Y_6WO_{12}:Eu$ powders. (a) Exciting into the host lattice and (b) into the $Eu^{3+}$ f-f transition**

**Table1　PL decay lifetime $t$ of $Eu^{3+}$ ions in the phosphors calcined at different temperatures $T$, $Ex$ and $Em$ are the excitation and emission wavelengths, respectively, $R^2$ is the adjusted R-square of the regression analysis of the decay data shown in Figure 7**

| $T$/℃ | $t$/ms | $R^2$ | $Ex$/nm | $Em$/nm | $t$/ms | $R^2$ | $Ex$/nm | $Em$/nm |
|---|---|---|---|---|---|---|---|---|
| 800 | 953(7) | 0.995 | 330 | 613 | 810(6) | 0.995 | 395 | 613 |
| 900 | 969(7) | 0.996 | 328 | 613 | 742(9) | 0.986 | 395 | 613 |
| 1 000 | 987(6) | 0.996 | 325 | 612 | 780(7) | 0.992 | 395 | 613 |
| 1 100 | 949(6) | 0.996 | 325 | 612 | 792(9) | 0.988 | 395 | 613 |
| 1 200 | 1 059(7) | 0.997 | 309 | 606 | 964(7) | 0.995 | 395 | 612 |
| 1 300 | 990(6) | 0.997 | 309 | 606 | 863(6) | 0.996 | 395 | 606 |

Generally speaking, $Eu^{3+}$ ions in different chemical environments should also show different decay

characters. The PL decay curves obtained by exciting the $WO_6$ groups and $Eu^{3+}$ ions of the samples are shown in Figure 7. It is revealed that all the curves can be well fitted to a first order exponential decay function,

$$I_t = I_0 + A\exp(-t/\tau) , \quad (2)$$

where $t$ is time, $\tau$ is the lifetime of the excitation state, $A$ is a constant, $I_t$ and $I_0$ are the PL intensity at time $t$ and $t=0$, respectively. By fitting the data to Eq. 2, the lifetimes of the emission are obtained and summarized in Table 1. It is observed that the lifetime varies in a narrow range from 0.949(6) ms to 1.059(7) ms, and generally increases with the calcination temperature in the cubic phase.

## 3 Conclusions

$Y_6WO_{12}:Eu^{3+}$ phosphors in cubic and rhombohedral phases were synthesized by a citrate-complexation based method. Red-emitting of $Eu^{3+}$ ions could be obtained under near-UV or blue light excitation. The excitation band of $WO_6$ in the near-UV region shifts from 309 of the rhombohedral to 330 nm of the cubic. At the same time, the red component in the emission increases gradually from rhombohedral to cubic and with the calcination temperature. The $Y_6WO_{12}:Eu^{3+}$ in cubic phase might be also promising near-UV excited red phosphors for solid-state lighting.

### Reference


[1] Bergh A, Craford G, Duggal A, et al. The Promise and Challenge of Solid-State Lighting [J]. Physics Today, 2001, 54: 42-47.

[2] Schubert E F, Kim J K, Luo H, et al. Solid-state lighting-a benevolent technology [J]. Rep Prog Phys, 2006, 69: 3069-3099.

[3] Schubert E F, Kim J K. Solid-State Light Sources Getting Smart [J]. Science, 2005, 308: 1274-1278.

[4] Yamada M, Naitou T, Izuno K, et al. Red-Enhanced White-Light-Emitting Diode Using a New Red Phosphor [J]. Jpn J Appl Phys, 2003, 42: L20-L23.

[5] Wang X, Zhang H, Zhao Y, et al. Effect of BN on Luminescent Properties of $Y_3Al_5O_{12}:Ce$ Phosphors and Their White LED Characteristics [J]. Int J Appl Ceram Technol, 2013, 10: 610-616.

[6] Li H, Zhou G, Xie R, et al. Optical Properties of Green-Blue-Emitting Ca-α-Sialon: $Ce^{3+}$, $Li^+$ Phosphors for White Light-Emitting Diodes (LEDs) [J]. J Solid State Chem, 2011, 184: 1036-1042.

[7] 钱先华，蒲锡鹏，张大凤，等. $NaY(WO_4)_2:Eu^{3+}$红色荧光粉的水热法制备及其发光性能研究[J]. 聊城大学学报(自然科学版)，2011 24(1): 74-77

[8] 史强，王长征，王利，等. ZnGa2O4 :Eu3＋红光荧光粉的光致及电致发光性能[J]. 聊城大学学报(自然科学版)，2010 32(1): 20-23.

[9] 宋兴旺，董国波，刘齐荣，等. 全薄膜电致变色器件 glass/ITO/NiOx/$ZrO_2$:H/$WO_3$/ITO 中单层膜的表征及器件的光学性能[J]. 聊城大学学报(自然科学版)，2016 29(1): 23-27

[10] Beaury O, Faucher M, Caro P. Crystal structure and fluorescence spectrum of $3Y_2O_3 \cdot WO_3:Eu^{3+}$[J]. Mater Res Bull, 1978, 13: 175-185.

[11] Li H, Yang H K, Moon B K, et al. Investigation of the structure and photoluminescence properties of $Eu^{3+}$ ion-activated $Y_6W_xMo_{(1-x)}O_{12}$[J]. J Mater Chem, 2011, 21: 4531-4537.

[12] Li H, Noh H M, Moon B K, et al. Wide-Band Excited $Y_6(WMo)_{0.5}O_{12}:Eu$ Red Phosphor for White Light Emitting Diode: Structure Evolution, Photoluminescence Properties, and Energy Transfer Mechanisms Involved [J]. Inorg Chem, 2013, 52: 11210-11217.

[13] Zheng Y, You H, Liu K, et al. Facile selective synthesis and luminescence behavior of hierarchical $NaY(WO_4)_2:Eu^{3+}$ and $Y_6WO_{12}:Eu^{3+}$[J]. CrystEngComm, 2011, 13: 3001-3007.

[14] Yu R, Shin D S, Jang K, et al. Photoluminescence Properties of Novel Host-Sensitized $Y_6WO_{12}:Dy^{3+}$ Phosphors [J]. J Am Ceram Soc, 2014, 97: 2170-2176.

[15] Yu R, Guo Y, Wang L, et al. Characterizations and optical properties of orange-red emitting $Sm^{3+}$-doped $Y_6WO_{12}$ phosphors [J]. J Lumin, 2014, 155: 317-321.

[16] Chien T C, Yang J C, Hwang C S, et al. Synthesis and photoluminescence properties of red-emitting $Y_6WO_{12}:Eu^{3+}$ phosphors [J]. J Alloys Compd, 2016, 676: 286-291.

[17] Bharat L K, Jeon Y I, Yu J S. $RE^{3+}$ ($RE^{3+}=Tm^{3+}$, $Tb^{3+}$ and $Sm^{3+}$) ions activated $Y_6WO_{12}$ phosphors: Synthesis, photoluminescence, cathodoluminescence and thermal stability [J]. J Alloys Compd, 2016, 685: 559-565.

[18] Bharat L K, Jeon Y I, Yu J S. Citrate-based sol - gel synthesis and luminescent properties of $Y_6WO_{12}:Eu^{3+}$, $Dy^{3+}$ phosphors for solid-state lighting applications [J]. Ceram Int, 2016, 42: 5677-5685.

[19] Diot N, Benard-Rocherulle P, Marchand R. X-ray powder diffraction data and Rietveld refinement for $Ln_6WO_{12}$ (Ln=Y, Ho) [J]. Powder Diffr, 2000, 15: 220-226.

[20] Aitken E A, Bartram S F, Juenke E F. Crystal chemistry of the rhombohedral $MO_3 \cdot 3R_2O_3$ compounds [J]. Inorg Chem, 1964, 3: 949-954.

[21] Borchardt H J. Yttrium-Tungsten Oxides [J]. Inorg Chem, 1963, 2: 170-173.

[22] Kiyoshi K, Masahiro Y, Tatsuo O, et al. High-Temperature Phase Relations in the System $Y_2O_3$-$Y_2O_3 \cdot WO_3$ [J]. J Am Ceram Soc, 1980, 63: 644-647.

[23] Yoshimura M, Ma J, Kakihana M. Low-Temperature Synthesis of Cubic and Rhombohedral $Y_6WO_{12}$ by a Polymerized Complex Method [J]. J Am Ceram Soc, 1998, 81: 2721-2724.

[24] Apostolov Z D, Sarin P, Hughes R W, et al. In Situ Synchrotron X-Ray Diffraction Study of the Rhombohedral-to-HT-Cubic Phase Transformation in $Ln_6WO_{12}$ (Ln=Y, Ho, Er, Yb) [J]. J Am Ceram Soc, 2014, 97: 1256-1263.

[25] Apostolov Z D, Sarin P, Haggerty R P, et al. In Situ Synchrotron X-Ray Diffraction Study of the Cubic to Rhombohedral Phase Transformation in $Ln_6WO_{12}$ (Ln=Y, Ho, Er, Yb) [J]. J Am Ceram Soc, 2013, 96: 987-994.

[26] Gagarina V A, Fomichev V V, Kondratov O I, et al. The calculation of vibrational spectra of heavy rare earth, yttrium and scandium molybdates and tungstates [J]. Russ J Inorg Chem, 1979, 24: 1856-1863.

[27] Chen L J, Su X, Wen J, et al. First-principles study of energetic and electronic properties of δ-$Re_6MO_{12}$ (Re=Ho, Gd, Y; M=U, W) [J]. J Appl Phys, 2013, 114: 083714.

[28] Li H, Pu X, Yin J, et al. Effect of Crystallite Size and Crystallinity on Photoluminescence Properties and Energy Transfer of $Y_6MoO_{12}$: Eu [J]. J Am Ceram Soc, 2016, 99: 954-961.

# 微观组织及晶体结构对 $Y_6WO_{12}:Eu^{3+}$ 荧光性能的影响

李怀勇　房　璐　李淼淼　孙文芝　位登虎　李　艳　马康熙　王雅妤

(聊城大学 材料科学与工程学院,山东 聊城 252059)

**摘　要**　本文采用柠檬酸复合物法合成了立方及菱方结构的 $Y_6WO_{12}:Eu^{3+}$ 多晶样品.采用 X-射线衍射、拉曼、稳态荧光及瞬态衰减测试手段对样品的晶体结构、荧光性能进行了表征.结果表明立方及菱方结构的荧光粉中的 $WO_6$ 基团和 $Eu^{3+}$ 离子分别可被近紫外光和蓝光所激发,但 $WO_6$ 基团在室温下不产生荧光.荧光粉的光致发光光谱以 $Eu^{3+}$ 离子的 $^5D_0$-$^7F_2$ 或 $^5D_0$-$^7F_1$ 跃迁所产生的红光发射为主.随着荧光粉焙烧温度及晶体结构的变化,荧光粉的激发、发射和瞬态衰减光谱相应的发生系统变化.本文从 $W^{6+}$ and $Eu^{3+}$ 离子晶体环境变化的角度对发光性能的变化进行了讨论.

**关键词**　钨酸盐;钪离子;荧光性能;能量传递

**中图分类号**　O644.1　　**文献标识码**　A